Prenatal THC exposure produces a hyperdopaminergic phenotype rescued by pregnenolone

Roberto Frau, PhD[1#], Vivien Miczán[2,3#], Francesco Traccis, MD[1], Sonia Aroni, PhD[1,4], Csaba I. Pongor, PhD[5], Pierluigi Saba[1], Valeria Serra[1], Claudia Sagheddu, PhD[1], Silvia Fanni, PhD[1], Mauro Congiu[1], Paola Devoto, PhD[1], Joseph F. Cheer, PhD[4], István Katona, PhD[3#], Miriam Melis, PhD[1*]

[1]Department of Biomedical Sciences, University of Cagliari, Cittadella Universitaria, Monserrato (CA), Italy; [2]Momentum Laboratory of Molecular Neurobiology, Institute of Experimental Medicine, Hungarian Academy of Sciences, Budapest, Hungary; [3]Faculty of Information Technology and Bionics, Pázmány Péter Catholic University, Budapest, Hungary; [4]Department of Anatomy and Neurobiology, University of Maryland School of Medicine, Baltimore, MD, United States of America; [5]Nikon Center of Excellence for Neuronal Imaging, Institute of Experimental Medicine, Hungarian Academy of Sciences, Budapest, Hungary.

[#]*These authors contributed equally to this work*

Corresponding Author:

Miriam Melis, PhD

Division of Neuroscience and Clinical Pharmacology

Department of Biomedical Sciences

University of Cagliari

Cittadella Universitaria

Monserrato (CA)

09042 -Italy

Email: myriam@unica.it

Tel: + 39 070 675 4322/4340

Mobile: +39 3498181954

Fax: +39 070 675 4320

Abstract

Increased legal availability of cannabis has led to a common misconception that it is a safe natural remedy for, amongst others, pregnancy-related ailments like morning sickness. Emerging clinical evidence, however, indicates that prenatal cannabis exposure (PCE) predisposes offspring to various neuropsychiatric disorders linked to aberrant dopaminergic function. Yet, our knowledge of how cannabis exposure affects the maturation of this neuromodulatory system remains limited. Here, we show that male, but not female, offspring of Δ^9-tetrahydrocannabinol (THC)-exposed dams, a rat PCE model, exhibit extensive molecular and synaptic changes in dopaminergic neurons of the ventral tegmental area, including altered excitatory-to-inhibitory balance and switched polarity of long-term synaptic plasticity. The resulting hyperdopaminergic state leads to increased behavioral sensitivity to acute THC during pre-adolescence. The FDA-approved neurosteroid pregnenolone rescues synaptic defects and normalizes dopaminergic activity and behavior in PCE offspring, suggesting a therapeutic approach for offspring exposed to cannabis during pregnancy.

Main text

The use of cannabis among pregnant women is increasing, with a prevalence rate of 3-16% in Western societies[1-4]. In association with the booming of cannabis marketing and the increased perception of its safety, cross-sectional analyses indicate that cannabis is often recommended to pregnant women as a treatment for morning sickness[5]. Although the use of medical cannabis for nausea and vomiting is approved in several states and countries, no legal distinction or warning for its use during pregnancy is mentioned[6]. Additionally, doctors or other health-care practitioners seldom advise pregnant women about the risks of taking cannabis during pregnancy[6, 7].

The main psychoactive ingredient of cannabis, Δ□-tetrahydrocannabinol (THC), interferes with the endocannabinoid system, which tightly controls progenitor cell proliferation and neuronal differentiation, axon growth and pathfinding, synapse formation and pruning in the developing brain[3, 8-10]. Accordingly, four independent longitudinal clinical studies demonstrated that prenatal cannabis exposure (PCE) predisposes to a wide array of behavioral and cognitive deficits including hyperactivity, enhanced impulsivity, loss of sustained attention, increased sensitivity to drugs of abuse[11-13] and susceptibility to psychosis[14]. Notably, all these neuropsychiatric impairments are tied to dysfunction of dopaminergic signaling[15, 16]. While the effects of acute and chronic cannabis use during adolescence and adulthood have been investigated[17-19], the impact of PCE on dopamine neurons within the ventral tegmental area (VTA), key players in motivation, reward and cognition[20], remains to be elucidated.

The “two-hit” model of psychiatric disorders posits that genetic background and/or environmental insults act as a “first hit”, perturbing brain development in a manner that leads to susceptibility to the onset of psychiatric symptoms upon a “second hit”. First hits can also lead to endophenotypes such as neurobehavioral deficits[21, 22], and characterizing

these may help to elucidate altered trajectories of circuit development that increase susceptibility to subsequent challenges[22, 23], which may in turn enable prevention of disease emergence. Notably, PCE was recently suggested to act as a “first hit” by interfering with the known complex developmental functions of endocannabinoid signaling, [3, 9, 23].

Longitudinal studies evaluating the behavioral effects of PCE on offspring have consistently shown increased impulsivity, increased incidence of risk-taking behaviors, and vulnerability to psychosis and enhanced sensitivity to drugs of abuse later in life, which can be detected as early as early infancy and throughout child development[11, 12, 14]. Furthermore, it is predicted that the ratio of affected children developing prenatal THC-induced endophenotypes is likely to be substantially higher[24, 25], but the complexity of uncontrollable genetic, environmental, and socioeconomic factors in humans makes the determination of causality very difficult. This highlights the advantage of animal models that mimic specific genetic and environmental factors. Here, we tested the hypothesis that PCE triggers molecular and synaptic changes in the VTA, leading to aberrant dopaminergic activity and behavioral susceptibility to subsequent challenges. In agreement with evidence that the first clinical neuropsychiatric symptoms manifest as early as infancy in PCE offspring[11, 14, 24], we find that prenatal THC exposure modeling PCE (hereafter referred to just as “PCE”) engenders “silent” functional abnormalities such as impaired sensorimotor gating, increased risk-taking and abnormal locomotor responses to THC in juvenile male offspring that become overt when acutely challenged with THC. Enhanced excitability of VTA dopamine neurons and larger THC-induced dopamine release accompany the PCE-induced endophenotype. Furthermore, we observe altered excitatory/inhibitory balance of VTA dopamine cells along with switched polarity from long-term depression to long-term potentiation at afferent excitatory synapses. Postnatal

administration of pregnenolone, a Federal Drug Agency (FDA)-approved drug, which is currently under investigation in clinical trials for cannabis use disorder, schizophrenia, autism and bipolar disorder (ClinicalTrials.gov Identifiers NCT00728728, NCT00615511, NCT02811939, NCT01881737, NCT02627508, NCT00223197, NCT01409096), normalized dopamine neuron excitability, restored synaptic properties and abnormal polarity of synaptic plasticity, as well as THC-induced dopamine release and deficits of sensorimotor gating functions.

Results

PCE induces a distinct behavioral endophenotype

To test the hypothesis that PCE triggers behavioral dysfunctions by altering midbrain dopaminergic activity, we modeled PCE by administering rat dams with THC (2 mg/kg s.c. once daily) during pregnancy (from gestational day 5 until 20). This low THC dose does not recapitulate behavioral responses in the cannabinoid tetrad assay or elicits cannabinoid tolerance after repeated administration[26], hence it represents a mild insult without any substantial direct impact on maternal behavior. We did not detect changes in litter size, maternal and non-maternal behavior, and in offspring body weight at this dose (**Supplementary Fig. 1**), indicating that malnutrition and maternal care did not account for any observed behavioral effects in the offspring. In terms of human consumption, this dose is equivalent to THC content in mild joints (5%)[27], since average THC content in illicit cannabis preparations has significantly increased in the last two decades (from ~4% to ~12%)[28].

To assess early signs of altered neurodevelopmental trajectories related to PCE endophenotypes, we tested offspring in a series of behavioral tasks, under basal

126 conditions and then following an acute THC (2.5 mg/kg s.c.) or vehicle (VEH) challenge
127 during the third and fourth postnatal week (postnatal day 15-28), corresponding to human
128 pre-adolescence. This is because in the “clinical staging model”, subclinical symptoms are
129 shown before adolescence and early adulthood[29], and a prominent research goal is the
130 identification of such endophenotypes[22]. Moreover, in healthy human subjects, cannabis
131 induces a wide range of deficits resembling the phenomenology of schizophrenia spectrum
132 disorders[19, 30]. Thus, we first investigated whether PCE alters sensorimotor gating
133 functions by using pre-pulse inhibition (PPI) of the acoustic startle reflex. Measures of
134 sensorimotor gating are among the most widely studied physiological markers used in
135 animal models of schizophrenia, and PPI deficits are present in patients with psychotic
136 disorders[31]. Notably, we found that PCE did not affect PPI *per se*. On the other hand, an
137 acute THC challenge disrupted PPI parameters in the PCE group but remained ineffective
138 in control (CTRL) offspring (**Fig. 1a**). Because this effect was sex-dependent and specific
139 for this developmental milestone (**Fig. 1b; Supplementary Fig. 2a**), all experiments
140 hereafter were carried out in male pre-adolescent rats. To test if PCE induces an
141 endophenotype associated with altered mesolimbic dopamine transmission, we next
142 performed in vivo cerebral microdialysis experiments in the shell of Nucleus Accumbens
143 (NAcS), one of the major target areas of midbrain VTA dopamine neurons
144 (**Supplementary Fig. 2b-d**). In accordance with our behavioral observations, we did not
145 detect alterations in basal extracellular dopamine levels, but the response to acute THC
146 administration was significantly larger in the PCE offspring group (**Fig. 1c**), indicating that
147 the mesolimbic dopamine system becomes sensitized following maternal THC use.
148 Moreover, we found that THC-induced disruption of PPI significantly and positively
149 correlated with the levels of dopamine in the NAcS (**Fig. 1d)** and required enhanced
150 mesolimbic dopamine signaling, because the inhibitor of tyrosine hydroxylase prevented
151 PPI deficits (**Fig. 1e**).

We next examined the effects of PCE on spontaneous locomotor responses to acute THC in an open field. No differences were observed between progenies, unless they were acutely treated with THC, as revealed by increased locomotor parameters (**Fig. 1f, Supplementary Fig. 3a,b**). These effects on spontaneous locomotion were causally dependent on VTA dopamine neuron function, because chemogenetic silencing of dopaminergic neurons by Gi-coupled DREADD (hM4Di) stimulation, counteracted the paradoxical hyperlocomotion elicited by THC in PCE offspring (**Fig. 1g, Supplementary Fig. 3c,d**). Next, we assessed whether the hyperlocomotion and reduced thigmotaxis observed in PCE after a single exposure to THC were associated to behavioral disinhibition. We tested the progenies in the dopamine-dependent suspended wire-beam bridge task, which measures the proclivity to engage in impulsive risk-taking behaviors. This task is operationally defined as the latency to access and move across an unstable bridge and to display stretched-attend postures, an ethologically relevant rodent behavior that occurs during risk assessment. PCE offspring were more prone to cross the bridge (**Fig. 1h**) and displayed a markedly impaired evaluation of risk assessment (**Fig. 1i**). Importantly, the propensity of PCE animals to take risks was not associated with alterations in emotional components, because progenies did not differ in the amount of defensive responses to sudden acoustic stimuli measured by startle amplitude (**Supplementary Fig. 3e**). Furthermore, they did not display differences in anxiety-related behavior assessed by the number of entries/time spent in open or closed arms, and in the number of transitions in the center on the elevated plus maze (**Supplementary Fig. 3f,g**).

PCE increases dopamine neuron excitability

We next determined the neurobiological mechanisms underlying heightened dopamine release associated with the behavioral susceptibility observed in PCE offspring. Because type-1 and type-2 cannabinoid (CB1 and CB2) receptors, molecular targets of THC,

regulate progenitor cell proliferation in the developing brain[8], we first investigated by confocal microscopy whether PCE alters the number of TH-positive cells or the intensity of TH-immunostaining in the VTA. Neither TH-positive dopamine neuron density (**Supplementary Fig. 4a-e**), nor TH levels measured in individual cells (**Supplementary Fig. 4f**) were different. We next probed the function of dopamine neurons by using whole-cell patch-clamp recordings to assess whether PCE-induced changes in physiological properties of dopaminergic neurons promote enhanced release. We performed current-clamp recordings in the lateral portion of the VTA, where cell bodies of the majority of dopamine neurons projecting to the NAcS reside[32], and we verified the TH-immunopositivity of the recorded neurons by post-hoc confocal microscopy. Dopamine neurons obtained from PCE offspring showed a different electrophysiological profile: they spontaneously fired at a higher frequency and displayed depolarized resting membrane potentials (**Fig. 2a-c**). Moreover, PCE dopamine neurons exhibited an overall increased excitability and higher maximum spiking frequencies in response to somatically injected currents (**Fig. 2d**). We also observed a reduced latency to action potential onset, the time needed for the first spike appearance in response to the smallest current injection (**Fig. 2e**). Moreover, a larger proportion of dopamine neurons fired action potentials (16/20, 80%) when compared to CTRL offspring (5/21 cells, ~23%; **Fig. 2e**) and showed enhanced spike fidelity (**Supplementary Fig. 5a-d**). This is consistent with decreased spike threshold in response to depolarizing current pulses in neurons from PCE slices (**Fig. 2f**). In contrast, we did not detect alterations in the after-hyperpolarization period following successive action potentials (**Fig. 2g-h**), in membrane capacitance or in inter-spike intervals (**Supplementary Fig. 5e,f**). Finally, PCE also modifies dopamine cell responses to acute THC by increasing spontaneous and evoked activity and enhancing spike fidelity in a dose- and CB1 receptor- dependent manner (**Supplementary Fig. 6**). Collectively, these results suggest that PCE biases the dopamine system by changing the

intrinsic properties of dopamine neurons and endowing them with a hyper-excitable phenotype, an underlying clinical feature of diverse psychiatric disorders[16, 20].

PCE shifts excitatory and inhibitory synaptic weights to dopamine neurons

To further address how PCE affects VTA dopamine neurons, we examined their synaptic properties. First, we observed a robust increase in the excitation-to-inhibition (E/I) ratio of dopamine neurons from PCE slices (**Fig. 3a**). To elucidate the underlying mechanisms of this phenomenon, we calculated AMPA/$GABA_A$ and NMDA/$GABA_A$ ratios (**Supplementary Fig. 7a-c**) and produced input-output curves from the responses measured at different stimulus intensities. A substantial decrease in synaptic inhibition of VTA dopamine cells obtained from PCE rats was revealed (**Fig. 3b**, **Supplementary Fig. 7a-c**). To assess whether this change arises from presynaptic mechanisms, we first computed the 1/coefficient of variation^2 ($1/CV^2$) value, which is an independent measure of changes in presynaptic function[33]. We found that PCE markedly decreases $1/CV^2$ of IPSCs at lower stimulus intensities indicating reduced release probability at inhibitory synapses (**Fig. 3c**). Additionally, PCE increased the paired-pulse ratio (PPR) of $GABA_A$ IPSCs (**Supplementary Fig. 7d,e**), and decreased the frequency, but not the amplitude of miniature IPSCs (mIPSCs) (**Supplementary Fig. 7f-h**).

Recent correlated electrophysiological and super-resolution imaging measurements have uncovered that the clustering of the cytomatrix protein bassoon in the presynaptic active zone is a reliable predictor of presynaptic release probability[34]. This is because augmented bassoon density inhibits the recruitment of voltage-gated calcium channels required for action potential-dependent vesicle release[34]. To identify the molecular substrates contributing to reduced synaptic inhibition of VTA dopamine cells from PCE animals, we combined confocal and stochastic optical reconstruction microscopy (STORM) and quantified bassoon density measured with nanometer precision within identified inhibitory

axon terminals impinging on the dendrites of dopamine neurons (**Fig. 3d**). We observed a substantial increase (by 45%) in the nanoscale density of bassoon at GABAergic synapses obtained from the PCE group (**Fig. 3e,f**, **Supplementary Fig. 8c**). In contrast, there was no change in the number and size of inhibitory boutons and their active zones, or in vesicular GABA transporter levels (**Supplementary Fig. 8**). Collectively, these data demonstrate that PCE induces a specific change in the presynaptic nanoarchitecture of inhibitory synapses and suggest that increased molecular crowding at vesicle release sites[34] contributes to the reduced synaptic inhibition of dopamine neurons.

CB1 receptors are among the most abundant metabotropic regulators of neurotransmitter release probability[35]. Compelling anatomical and electrophysiological evidence shows that CB1 activation decreases GABA release thereby sculpting the activity of dopamine signaling[36, 37]. Therefore, we tested the hypothesis that enhanced cannabinoid receptor control at inhibitory synapses contributes to reduced synaptic inhibition. The mixed CB1/CB2 receptor agonist WIN 55,212-2 (WIN) produced a larger and faster effect on evoked IPSC amplitude recorded from VTA dopamine cells in PCE offspring (**Fig. 3g-i**). However, STORM imaging showed no difference in CB1 levels at GABAergic afferents to dopamine neurons (**Fig. 3j**). These nanoscale super-resolution data together indicate that the ratio of the presynaptic regulatory CB1 receptors and their molecular effectors in the release machinery complex shifted so that less voltage-gated calcium channels are controlled by a similar number of CB1 receptors on inhibitory axon terminals in the PCE group versus the CTRL group. This implies that a saturating dose of the CB1 agonist WIN should have the same effects on $GABA_A$ IPSC amplitude, and that WIN effects on IPSCs should be faster, which was in fact the case (**Fig. 3i**). Altogether, these findings demonstrate that PCE induces a molecular reorganization of the active zone leading to

increased presynaptic cannabinoid control along with markedly reduced GABAergic inhibition.

To gain insights into the consequences of PCE on excitatory synaptic transmission, we first measured input-output curves from responses elicited at different stimulus intensities. We found that a larger stimulus intensity is required to recruit the same magnitude of synaptic excitation indicating that PCE induces reduction in the number and/or strength of excitatory inputs terminating on dopamine neurons (**Fig. 4a**). Indeed, confocal microscopy analysis uncovered a robust (~50%) reduction in the density of type I vesicular glutamate transporter (vGluT1)-positive excitatory axon terminals contacting TH-positive dopaminergic neurons in the lateral VTA (**Supplementary Fig. 9a-c**). On the other hand, there were no differences in the $1/CV^2$ values of EPSCs (**Fig. 4b**), in their PPR (**Supplementary Fig. 9d,e)** or in the frequency of mEPSCs (**Supplementary Fig. 9f,g**). In contrast to the lack of presynaptic physiological changes, we observed an increased amplitude of mEPSCs (**Supplementary Fig. 9f,h**) and longer decay kinetics of postsynaptic AMPA currents (**Fig. 4c**), indicating that PCE affected the post-synaptic responsiveness of afferent excitatory synapses of VTA dopamine neurons. Likewise, PCE elicited a larger AMPA/NMDA ratio with the frequency distribution curve shifted to the right in dopamine cells of PCE offspring (**Fig. 4d-f**). Notably, similar increases in the AMPA/NMDA ratio are observed in VTA dopamine neurons of offspring exposed in utero to cocaine or alcohol[38, 39]. Thus, potentiated AMPA/NMDA ratios in the postnatal PCE brain directly reflects prenatal drug exposure. We also computed NMDA EPSC decay time kinetics, measured as weighted tau (τ), and found that they were faster in neurons recorded from the PCE progeny (**Fig. 5a,b**), and were more sensitive to GluN2A blockade (**Fig. 5c**), indicative of an increased ratio GluN2A/N2B subunits in NMDA receptors[38]. Next, we examined the current-voltage relationship (I–V) of AMPA EPSCs. When

277 compared to CTRL animals, PCE offspring I-V curves were non-linear, exhibited inward
278 rectification (**Fig. 5d,e**) and the GluA2 blocker NASPM reduced AMPA EPSCs to a larger
279 extent (**Fig. 5f**), indicating the insertion of calcium permeable (i.e., GluA2-lacking) AMPA
280 receptors[38, 39]. Taken together, these microscopic and electrophysiogical results suggest
281 that PCE delays the molecular and anatomical maturation of excitatory synaptic inputs on
282 VTA dopaminergic neurons, leading to increased postsynaptic responsiveness, a well-
283 known property of developing brain circuits.

284 A major consequence of reduced inhibitory control of dopamine neurons together with
285 heightened responsiveness to their excitatory inputs might also be a shift in the threshold
286 for synaptic plasticity induction. Pairing low-frequency presynaptic stimulation (LFS, 1 Hz)
287 with post-synaptic membrane depolarization (-40 mV) resulted in the expected long-term
288 depression (LTD) of excitatory synapses[40]. In contrast, we found that the very same
289 stimulus protocol elicited a marked long-term potentiation (LTP) in VTA dopamine neurons
290 from PCE animals (**Fig. 5g,h**), an effect reminiscent of immature glutamatergic synapses.

291 We next examined whether the synaptic effects of PCE were cell-type-specific in the
292 lateral VTA circuitry. GABA and dopamine neurons, which make up the vast majority of
293 neurons in the lateral VTA[41] (**Supplementary Fig. 10a,b**), could be reliably distinguished
294 by their morphological and electrophysiological characteristics and by the absence or
295 presence of TH[42] in post-hoc immunofluorescence analysis, respectively (**Supplementary**
296 **Fig. 10c-l**). While PCE did not affect E/I balance, it decreased the AMPA/NMDA ratio
297 (**Supplementary Fig.11a,b**). Notably, NMDA EPSC decay time, I-V of AMPA EPSCs,
298 PPR of both AMPA EPSCs and $GABA_A$ IPSCs in putative GABA cells did not differ
299 between progenies (**Supplementary Fig.11c-f**). Thus, PCE does not alter the content of
300 GluA2-containing AMPARs and GluN2A-containing NMDARs at these synapses onto VTA
301 putative GABA neurons but specifically modifies EPSC generation. Collectively, these

findings suggest that PCE predominantly affects the synaptic maturation of dopamine cells within the VTA circuitry.

Pregnenolone rescues dopamine function and behavior after PCE

Since preventative strategies to reduce the burden of PCE in offspring are currently not in place[7], the identification of the PCE endophenotype is instrumental to test therapeutic interventions during prodromal phases of late-onset psychiatric disorders. Particularly, early interventions are needed prior to the time point at which PCE offspring manifest the age of risk for a disorder to prevent phenoconversion to late-onset disease[14, 29, 43] .

The FDA-approved neurosteroid pregnenolone (PREG) reverses behaviors such as psychomotor agitation and deficits in PPI that are observed in individuals with schizophrenia [44]. Notably, it also acts as a negative regulator of CB1 receptor signaling[45]. Therefore, we predicted that a short postnatal treatment of PCE offspring with PREG would be a good candidate for reversing PCE-induced changes in the properties of VTA dopamine neurons and behavior. To assess this, we administered PREG (6 mg/kg s.c. once daily for 9 days, from PND 15 to 23) to VEH or PCE offspring, and acute VTA-containing slices were prepared 1 and 2 days following the last administration (**Fig. 6a**), when PREG is cleared from the brain. Remarkably, PREG rescued LTD at excitatory synapses on dopamine neurons to CTRL levels (**Fig. 6b**), without affecting synaptic efficacy in CTRL offspring. Moreover, PREG ameliorated PCE-induced dopamine neuron excitability in PCE slices, measured by resting membrane potential (**Fig. 6c**), as well as spontaneous (**Fig. 6d-f**) and evoked firing activity (**Fig. 6g,h**). PREG also fully restored the alterations in synaptic properties imposed by PCE on excitatory and inhibitory inputs on dopamine cells (**Supplementary Fig. 12**). Most importantly, PREG selectively prevented larger acute THC-induced enhancement of dopamine levels in NAcS (**Fig. 6i,j**), and THC-induced disruption of somatosensory gating functions in PCE offspring (**Fig. 6k**). Finally,

we found that PREG mechanism of action was dissociated from its downstream neurosteroid metabolites (**Supplementary Fig.13**). Collectively, these results indicate that PREG prevents PCE-induced hyperdopaminergic states and confers resilience towards heightened acute effects of THC in PCE animals.

Discussion

In the present study, we provide evidence that maternal THC exposure induces multifaceted molecular, cellular and synaptic adaptations that converge into aberrant dopamine function in juvenile male rat offspring. Such persistently enhanced excitability of VTA dopamine neurons is a well-established neurodevelopmental risk factor conferring biased dopamine transmission and vulnerability to discrete psychiatric disorders. This might manifest in aberrant associative learning and abnormal reward processing, and provide an interpretative framework for clinical studies reporting maladaptive behaviors, ranging from affective dysregulation to psychosis and addiction vulnerability in the offspring of mothers using cannabis during pregnancy[3, 11, 14]. It is possible that the decreased expression of dopamine D2 receptors observed in human PCE offspring amygdala and nucleus accumbens[46, 47] may be an adaptive response elicited by this hyperdopaminergic state, and may also contribute to the vulnerability to psychiatric disorders[15].

We propose that the hyperdopaminergic state and the activity-dependent synapse-specific remodeling identified in the present study are significant neurobiological substrates, which may promote a susceptible endophenotype conferred by maternal cannabis use. This is important because preclinical and clinical studies have also established a prominent and causative role for mesostriatal dopamine dysfunction, in particular elevated dopamine synthesis and release properties, in the pathophysiology of schizophrenia[16]. Notably,

positron emission tomography imaging studies have linked genetic risk for THC-induced psychosis to differential increases of dopamine release by THC[48], a phenomenon exhibiting a high degree of familiarity[49], raising the possibility that PCE offspring represent one proportion of cannabis users vulnerable for THC-induced psychosis[50]. Hence, PCE might be a risk factor conferring increased vulnerability to psychotic experiences as early as childhood[14]. Since PCE-induced dopamine dysregulation may predispose to THC-dependent delusions and hallucinations, PCE may represent a relevant modifiable predictor of transition to psychotic disorder.

Our findings are consistent with the protective actions of pregnenolone in acute THC intoxication in rodents[45], and in an established mouse model for schizophrenia[44] as a negative regulator of CB1 signaling. Although pregnenolone metabolites such as progesterone may have direct effects on GABA and NMDA receptors, the observation that inhibition of the converting enzyme 3β-hydroxysteroid dehydrogenase did not modify the protective effects of pregnenolone on PPI disruption induced by acute THC is consistent with the possibility that pregnenolone *per se* ameliorates PCE-induced physiological and behavioral dysfunctions. Since pregnenolone is a well-tolerated FDA-approved drug, devoid of major side effects[45], our pharmacological treatment has high translational value as a safe and promising therapeutic approach for offspring of mothers who abused marijuana during pregnancy. Our study warrants further investigation into the effects of PCE on other anatomically and functionally heterogeneous dopamine subpopulations with different axonal projections. Indeed, since our recordings were carried out from the lateral portion of the VTA, which largely projects to the lateral shell of the NAc[32], it is likely that these dopamine neurons would mainly project to this region.

Finally, it is important to emphasize that some of the potentiated state measures of dopamine neurons resemble those described in VTA dopamine neurons of offspring

exposed in utero to cocaine or alcohol[38, 39]. As physicians caution pregnant women to not use alcohol and cocaine because of their detrimental effects to the fetus, based on our findings, it is our recommendation that they also advise them on the consequences of the use of cannabis during pregnancy. Considering that such preventative strategies do not take place due to the underestimation of the risks of neurodevelopmental adverse effects associated with maternal cannabis use[6, 7], and that cannabis legalization policies move forward worldwide and conceivably large numbers of children will be prenatally exposed to its ingredients over the next decades, the present findings are critically important for unmasking and highlighting extensive neurobiological maladaptations that increase the vulnerability of at-risk offspring to neuropsychiatric disorders.

References

1. Administration, S.A.a.M.H.S. Results from the 2010 National Survey on Drug Use and Health: Summary of National Findings. (ed. S.A.a.M.H.S. Administration.) (Rockville, MD, 2011).
2. Addiction, E.M.C.f.D.a.D. European Monitoring Centre for Drugs and Drug Addiction (2012): Legal topic overviews: Possession of cannabis for personal use. EMCDDA. . (2012).
3. Alpar, A., Di Marzo, V. & Harkany, T. At the Tip of an Iceberg: Prenatal Marijuana and Its Possible Relation to Neuropsychiatric Outcome in the Offspring. *Biol Psychiatry* **79**, e33-45 (2016).
4. Brown, Q.L.*, et al.* Trends in Marijuana Use Among Pregnant and Nonpregnant Reproductive-Aged Women, 2002-2014. *Jama* **317**, 207-209 (2017).
5. Dickson, B.*, et al.* Recommendations From Cannabis Dispensaries About First-Trimester Cannabis Use. *Obstet Gynecol* **131**, 1031-1038 (2018).
6. Volkow, N.D., Compton, W.M. & Wargo, E.M. The Risks of Marijuana Use During Pregnancy. *Jama* **317**, 129-130 (2017).
7. Jansson, L.M., Jordan, C.J. & Velez, M.L. Perinatal Marijuana Use and the Developing Child. *Jama* (2018).
8. Galve-Roperh, I.*, et al.* Cannabinoid receptor signaling in progenitor/stem cell proliferation and differentiation. *Prog Lipid Res* **52**, 633-650 (2013).
9. Maccarrone, M., Guzman, M., Mackie, K., Doherty, P. & Harkany, T. Programming of neural cells by (endo)cannabinoids: from physiological rules to emerging therapies. *Nat Rev Neurosci* **15**, 786-801 (2014).
10. Wu, C.S., Jew, C.P. & Lu, H.C. Lasting impacts of prenatal cannabis exposure and the role of endogenous cannabinoids in the developing brain. *Future Neurol* **6**, 459-480 (2011).

11. Morris, C.V., DiNieri, J.A., Szutorisz, H. & Hurd, Y.L. Molecular mechanisms of maternal cannabis and cigarette use on human neurodevelopment. *Eur J Neurosci* **34**, 1574-1583 (2011).
12. Huizink, A.C. Prenatal cannabis exposure and infant outcomes: overview of studies. *Prog Neuropsychopharmacol Biol Psychiatry* **52**, 45-52 (2014).
13. De Genna, N.M., Richardson, G.A., Goldschmidt, L., Day, N.L. & Cornelius, M.D. Prenatal exposures to tobacco and cannabis: Associations with adult electronic cigarette use. *Drug Alcohol Depend* **188**, 209-215 (2018).
14. Fine, J.D.*, et al.* Association of Prenatal Cannabis Exposure With Psychosis Proneness Among Children in the Adolescent Brain Cognitive Development (ABCD) Study. *JAMA Psychiatry* (2019).
15. Volkow, N.D., Fowler, J.S., Wang, G.J. & Swanson, J.M. Dopamine in drug abuse and addiction: results from imaging studies and treatment implications. *Mol Psychiatry* **9**, 557-569 (2004).
16. Grace, A.A. Dysregulation of the dopamine system in the pathophysiology of schizophrenia and depression. *Nat Rev Neurosci* **17**, 524-532 (2016).
17. Bloomfield, M.A., Ashok, A.H., Volkow, N.D. & Howes, O.D. The effects of Delta9-tetrahydrocannabinol on the dopamine system. *Nature* **539**, 369-377 (2016).
18. Bourque, J., Afzali, M.H. & Conrod, P.J. Association of Cannabis Use With Adolescent Psychotic Symptoms. *JAMA Psychiatry* **75**, 864-866 (2018).
19. Di Forti, M.*, et al.* The contribution of cannabis use to variation in the incidence of psychotic disorder across Europe (EU-GEI): a multicentre case-control study. *Lancet Psychiatry* (2019).
20. Buckholtz, J.W.*, et al.* Mesolimbic dopamine reward system hypersensitivity in individuals with psychopathic traits. *Nat Neurosci* **13**, 419-421 (2010).
21. Geschwind, D.H. & Flint, J. Genetics and genomics of psychiatric disease. *Science* **349**, 1489-1494 (2015).
22. Insel, T.R. Rethinking schizophrenia. *Nature* **468**, 187-193 (2010).
23. Heffernan, A.L. & Hare, D.J. Tracing Environmental Exposure from Neurodevelopment to Neurodegeneration. *Trends Neurosci* **41**, 496-501 (2018).
24. Richardson, K.A., Hester, A.K. & McLemore, G.L. Prenatal cannabis exposure - The "first hit" to the endocannabinoid system. *Neurotoxicol Teratol* **58**, 5-14 (2016).
25. Young-Wolff, K.C.*, et al.* Trends in Self-reported and Biochemically Tested Marijuana Use Among Pregnant Females in California From 2009-2016. *Jama* **318**, 2490-2491 (2017).
26. Wiley, J.L., O'Connell M, M., Tokarz, M.E. & Wright, M.J., Jr. Pharmacological effects of acute and repeated administration of Delta(9)-tetrahydrocannabinol in adolescent and adult rats. *J Pharmacol Exp Ther* **320**, 1097-1105 (2007).
27. Mehmedic, Z.*, et al.* Potency trends of Delta9-THC and other cannabinoids in confiscated cannabis preparations from 1993 to 2008. *J Forensic Sci* **55**, 1209-1217 (2010).
28. ElSohly, M.A.*, et al.* Changes in Cannabis Potency Over the Last 2 Decades (1995-2014): Analysis of Current Data in the United States. *Biol Psychiatry* **79**, 613-619 (2016).
29. McGorry, P.D., Hickie, I.B., Yung, A.R., Pantelis, C. & Jackson, H.J. Clinical staging of psychiatric disorders: a heuristic framework for choosing earlier, safer and more effective interventions. *Aust N Z J Psychiatry* **40**, 616-622 (2006).
30. Sherif, M., Radhakrishnan, R., D'Souza, D.C. & Ranganathan, M. Human Laboratory Studies on Cannabinoids and Psychosis. *Biol Psychiatry* **79**, 526-538 (2016).
31. Braff, D.L., Swerdlow, N.R. & Geyer, M.A. Gating and habituation deficits in the schizophrenia disorders. *Clin Neurosci* **3**, 131-139 (1995).

32. Lammel, S., Ion, D.I., Roeper, J. & Malenka, R.C. Projection-specific modulation of dopamine neuron synapses by aversive and rewarding stimuli. *Neuron* **70**, 855-862 (2011).
33. Malinow, R. & Tsien, R.W. Presynaptic enhancement shown by whole-cell recordings of long-term potentiation in hippocampal slices. *Nature* **346**, 177-180 (1990).
34. Glebov, O.O.*, et al.* Nanoscale Structural Plasticity of the Active Zone Matrix Modulates Presynaptic Function. *Cell Rep* **18**, 2715-2728 (2017).
35. Lovinger, D.M. Presynaptic modulation by endocannabinoids. *Handb Exp Pharmacol*, 435-477 (2008).
36. Matyas, F.*, et al.* Identification of the sites of 2-arachidonoylglycerol synthesis and action imply retrograde endocannabinoid signaling at both GABAergic and glutamatergic synapses in the ventral tegmental area. *Neuropharmacology* **54**, 95-107 (2008).
37. Melis, M.*, et al.* Enhanced endocannabinoid-mediated modulation of rostromedial tegmental nucleus drive onto dopamine neurons in Sardinian alcohol-preferring rats. *The Journal of neuroscience : the official journal of the Society for Neuroscience* **34**, 12716-12724 (2014).
38. Bellone, C., Mameli, M. & Luscher, C. In utero exposure to cocaine delays postnatal synaptic maturation of glutamatergic transmission in the VTA. *Nat Neurosci* **14**, 1439-1446 (2011).
39. Hausknecht, K.*, et al.* Excitatory synaptic function and plasticity is persistently altered in ventral tegmental area dopamine neurons after prenatal ethanol exposure. *Neuropsychopharmacology* **40**, 893-905 (2015).
40. Thomas, M.J., Malenka, R.C. & Bonci, A. Modulation of long-term depression by dopamine in the mesolimbic system. *The Journal of neuroscience : the official journal of the Society for Neuroscience* **20**, 5581-5586 (2000).
41. Yamaguchi, T., Sheen, W. & Morales, M. Glutamatergic neurons are present in the rat ventral tegmental area. *Eur J Neurosci* **25**, 106-118 (2007).
42. Chieng, B., Azriel, Y., Mohammadi, S. & Christie, M.J. Distinct cellular properties of identified dopaminergic and GABAergic neurons in the mouse ventral tegmental area. *J Physiol* **589**, 3775-3787 (2011).
43. Marin, O. Developmental timing and critical windows for the treatment of psychiatric disorders. *Nat Med* **22**, 1229-1238 (2016).
44. Wong, P., Sze, Y., Chang, C.C., Lee, J. & Zhang, X. Pregnenolone sulfate normalizes schizophrenia-like behaviors in dopamine transporter knockout mice through the AKT/GSK3beta pathway. *Transl Psychiatry* **5**, e528 (2015).
45. Vallee, M.*, et al.* Pregnenolone can protect the brain from cannabis intoxication. *Science* **343**, 94-98 (2014).
46. Wang, X., Dow-Edwards, D., Anderson, V., Minkoff, H. & Hurd, Y.L. In utero marijuana exposure associated with abnormal amygdala dopamine D2 gene expression in the human fetus. *Biol Psychiatry* **56**, 909-915 (2004).
47. DiNieri, J.A.*, et al.* Maternal cannabis use alters ventral striatal dopamine D2 gene regulation in the offspring. *Biol Psychiatry* **70**, 763-769 (2011).
48. Kuepper, R.*, et al.* Delta-9-tetrahydrocannabinol-induced dopamine release as a function of psychosis risk: 18F-fallypride positron emission tomography study. *PLoS One* **8**, e70378 (2013).
49. McGrath, J.*, et al.* Association between cannabis use and psychosis-related outcomes using sibling pair analysis in a cohort of young adults. *Arch Gen Psychiatry* **67**, 440-447 (2010).
50. Compton, M.T.*, et al.* Association of pre-onset cannabis, alcohol, and tobacco use with age at onset of prodrome and age at onset of psychosis in first-episode patients. *Am J Psychiatry* **166**, 1251-1257 (2009).

515

516

Materials and Methods

Animals. All procedures were performed in accordance with the European legislation EU Directive 2010/63 and the National Institute of Health Guide for the Care and Use of Laboratory Animals and were approved by the Animal Ethics Committees of the University of Cagliari and by Italian Ministry of Health (auth. n. 659/2015-PR and 725/2019-PR) and by the Institutional Animal Use and Care Committee at the University of Maryland (0617002), Baltimore. We made all efforts to minimize pain and suffering and to reduce the number of animals used. Primiparous female Sprague Dawley (Envigo) rats (bred with males) were used as mothers and single housed during pregnancy. Long Evans dams expressing cre recombinase under the control of the tyrosine hydroxylase (TH) promoter (TH::Cre) were used for DREADDs experiments. Δ^9-tetrahydrocannabinol (THC) or vehicle was administered (2 mg kg-1 2 ml kg-1s.c. once per day) from gestational day 5 (GD5) until GD20. Offspring were weaned at ~PND21 and maintained without any further manipulation in standard conditions of temperature (21 ± 1°C) and humidity (60%) on normal 12-h light/dark cycle with *ad libitum* access to food and water until the experimental day (PND 15-28). We did not use more than two males from each litter for the same experiment, to control for litter effect. All the additional male pups in each litter were used for other experiments (i.e. cerebral microdialysis, behavioral paradigms, STORM analysis, different electrophysiological protocols), in order to minimize the total number of animals.

Surgical procedures

TH::Cre positive offspring were stereotaxically injected under isoflurane (3% induction, 1-2% maintenance) with a cre-dependent adeno-associated virus expressing an inhibitory DREADD construct (AAV5-DIO-hM4D(Gi)-mCherry, PCE-Gi), or control virus (AAV5-DIO-mCherry, PCE) to target dopamine neurons in the ventral tegmental area (VTA) at postnatal day 7 (PND7). Viruses were injected at a volume of 0.5 µl/side and rate of

0.1 µl/min in the VTA (AP -4.2, LM ± 0.6 mm from bregma, and DV -5.25 mm from cortical surface) with a Hamilton syringe. Injection needles were left in place for 5 mins after the injection to assure adequate viral delivery.

Behavioral analyses

Maternal behavior observation. The behavior of each dam was assessed from PND 1 to PND 20 by an observer blind to the experimental groups until the analysis of data. The observation was performed five times per day at 9:00, 11:30, 13:30, 15:00 and 17:00 during the light phase (lights on at 7:00) and consisted of 3 trials of instantaneous observation for a total of 15 observations per day and a total 300 observations per dam. As behavioral parameters: retrieval, arched-back, blanket and passive nursing, pup licking (regarded as maternal behaviors), self-grooming, eating, drinking, rearing, moving, resting, standing out of the nest (considered as non-maternal behaviors) were scored. Observation strictly followed the previously published detailed analysis[51]. Briefly, the behaviors were recorded using dichotomous scores (0/1): 0 was assigned when the behavior was not present, whereas it was scored as, 1 when it was present. Data were expressed as percentage of observation of maternal or non-maternal behavior.

Startle reflex and Pre-pulse Inhibition. Startle reflex and Pre-pulse Inhibition (PPI) were tested as previously described[52]. Briefly, the apparatus (Med Associates) consisted of four standard cages placed in sound-attenuated chambers with fan ventilation. Each cage consisted of a Plexiglas cylinder of 5 cm diameter, mounted on a piezoelectric accelerometric platform connected to an analog-digital converter. Two separate speakers conveyed background noise and acoustic bursts, each one properly placed so as to produce a variation of sound within 1 dB across the startle cage. Both speakers and startle cages were connected to a main PC, which detected and analyzed all chamber variables with specific software. Before each testing session, acoustic stimuli and mechanical responses were calibrated via specific devices supplied by Med Associates. The testing

session featured a background noise of 70 dB and consisted of an acclimatization period of 5 min, followed by three consecutive sequences of trials (blocks). Unlike the first and the third block, during which rats were presented with only five pulse-alone trials of 115 dB, the second block consisted of a pseudorandom sequence of 50 trials, including 12 pulse-alone trials, 30 trials of pulse preceded by 74, 78, or 86 dB pre-pulses (10 for each level of pre-pulse loudness), and eight no-stimulus trials, where only the background noise was delivered. Inter-trial intervals were selected randomly between 10 and 15 s. The % PPI value was calculated using the following formula: 100 − [(mean startle amplitude for pre-pulse pulse trials/mean startle amplitude for pulse alone trials)*100]. PPI values related to different prepulse levels were collapsed, given that no interactions were found between pre-pulse levels throughout the study.

Locomotor activity. Locomotor behaviors of Sprague Dawley and Long Evans TH::Cre rats were tested in two different facilities at the University of Cagliari (Italy) and at the University of Maryland School of Medicine (USA), respectively. Rats were placed in the center of a novel square open field (dimension: 42 x 42 x 30 cm, L x W x H) and their behavior was monitored for 40 min and collected every 10 minutes. Analysis of locomotor activity of Sprague Dawley and Long Evans TH::Cre rats were performed by using Omnitech Digiscan monitoring system (Omnitech Digiscan cages; Columbus, OH, USA) and Ethovision (Noldus Instruments, Wageningen, The Netherlands), respectively. Behavioral measurements included the assessment of the total distance traveled (cm), and the periphery and center time, respectively calculated as the durations of time spent along the perimeter of the walls (a 20-cm-wide external square frame) or in the center of the arena (an internal square measuring 20 x 20 cm). To minimize differences in baseline spontaneous locomotor activity (i.e., distance travelled), we normalized the data to their reference group (e.g., CTRL-VEH and PCE-VEH). For DREADD experiments, open field

593 testing was performed 30 minutes following systemic administration of clozapine-N-oxide
594 (CNO, 3 mg/kg/2 ml i.p.) to engage VTA Gi-DREADDs.
595 *Elevated plus-maze*. The test was performed as previously described[53]. Briefly, we used a
596 black Plexiglas apparatus consisting of two opposing open arms (length: 40 cm, width: 9
597 cm) and two closed arms (wall height: 15 cm), which extended from a central square
598 platform (9 × 9 cm), positioned 70 cm from the ground. Rats were individually placed on
599 the central platform facing the open arm. Behavior was recorded for 5 min. Measures
600 included: entries and duration in the open and closed arms and the central platform;
601 frequency of stretch-attend postures and head dips (defined as previously described).
602 *Wire-beam bridge test.* Testing was performed on a variant of the protocol previously
603 detailed[54, 55], specifically adapted for rats. The apparatus consists of two 156 cm high
604 Plexiglas platforms, connected by a horizontal, flexible wire-beam (100 cm long). A 52-cm
605 high Plexiglas wall was placed on the proximity of the edge (3 cm from the edge) of one
606 platform, in order to make the starting position uncomfortable and promote movement. The
607 bridge consisted of 2 parallel beams (0.1 cm thick) perpendicularly connected by 34
608 equally distanced cross-ties (3 cm long). It was modestly flexible, with a downward
609 deflection of 2 cm per 100-g load at the center point. Rats were individually placed in the
610 start position and the latency to cross and reach the other platform was recorded. The
611 duration of overall immobility and number of crossings on ties were also monitored.
612 *Cerebral microdialysis.* Rats were anesthetized with Equithesin and placed in a Kopf
613 stereotaxic apparatus. In-house constructed vertical microdialysis probes (AN 69-HF
614 membrane, Hospal-Dasco; cut-off 40,000 Dalton, 3 mm dialyzing membrane length) were
615 implanted in the nucleus accumbens shell (AP: +1.5, L: ±0.7, V: -7.0 from bregma)
616 according to atlas coordinates[56], empirically corrected after pilot experiment. Rats were
617 given antibiotic therapy (enrofloxacin, Bayer HealthCare, Shawnee Mission, KS) and
618 allowed to recover in their home cages before testing. The day after probe implantation,

artificial cerebrospinal fluid solution (aCSF; 147 mM NaCl, 4 mM KCl, 1.5 mM $CaCl_2$, 1 mM $MgCl_2$, pH 6-6.5) was pumped through the dialysis probes at a constant rate of 1.1 µl min-1 via a CMA/100 microinjection pump (Carnegie Medicine). Samples were collected every 20 min and immediately analyzed for dopamine content by HPLC with electrochemical detection, as previously described[57]. When a stable baseline was obtained (three consecutive samples with a variance not exceeding 15%), THC (2.5 mg kg-1, 2 ml kg-1) was i.p. administered and sample collection continued for two hours. On completion of the testing, rats were sacrificed by Equithesin overdose, the brains were removed and sectioned by a cryostat (Leica CM3050 S) in 40 µm thick coronal slices to verify the anatomical locations of dialysis probes.

Electrophysiological recordings. The preparation of VTA slices was performed as described previously[67]. Briefly, a block of tissue containing the midbrain was obtained from male offspring deeply anesthetized with isoflurane and sliced in the horizontal plane (300 µm) with a vibratome (Leica) in ice-cold low-Ca^{2+} solution containing the following (in mM): 126 NaCl, 1.6 KCl, 1.2 NaH_2PO_4, 1.2 $MgCl_2$, 0.625 $CaCl_2$, 18 $NaHCO_3$, and 11 glucose. Slices were transferred to a holding chamber with aCSF (37°C) saturated with 95% O_2 and 5% CO_2 containing the following (in mM): 126 NaCl, 1.6 KCl, 1.2 NaH_2PO_4, 1.2 $MgCl_2$, 2.4 $CaCl_2$, 18 $NaHCO_3$, and 11 glucose. Slices were allowed to recover for at least 1 h before being placed, as hemislices, in the recording chamber and superfused with aCSF (36-37°C) saturated with 95% O_2 and 5% CO_2. Cells were visualized with an upright microscope with infrared illumination (Axioskop FS 2 plus; Zeiss), and whole-cell patch-clamp recordings were made by using an Axopatch 200B amplifier (Molecular Devices). Recordings were carried out in the lateral portion of the VTA (**supplementary Fig. 10a,b**). Voltage-clamp recordings of evoked inhibitory postsynaptic currents (IPSCs) and current-clamp recordings were made with electrodes filled with a solution containing (in mm): 144 KCl, 10 HEPES, 3.45 BAPTA, 1 $CaCl_2$, 2.5 Mg_2ATP, and 0.25 Mg_2GTP, pH 7.2–7.4, 275–

285 mOsm. All $GABA_A$ IPSCs were recorded in the presence of 2-amino-5-phosphonopentanoic acid (AP5; 100 µm), 6-cyano-2,3-dihydroxy-7-nitro-quinoxaline (10 µm), strychnine (1 µm), and eticlopride (100 nm) to block NMDA, AMPA, glycine, and dopamine D2-mediated synaptic currents, respectively. As described previously[68], this solution had no effect on the holding current of the dopamine cells. Current-clamp experiments were performed in the absence of any pharmacological blocker, i.e., in regular aCSF. Experiments were begun only after series resistance had stabilized (typically 10–30 MΩ), which was monitored by a hyperpolarizing step of −4 mV at each sweep, every 10 s. Data were excluded when the resistance changed >20%. Voltage-clamp recordings of evoked excitatory PSCs (EPSCs) were made with electrodes filled with a solution containing (in mm): 117 Cs methansulfonic acid, 20 HEPES, 0.4 EGTA, 2.8 NaCl, 5 TEA-Cl, 0.1 mM spermine, 2.5 Mg_2ATP, and 0.25 Mg_2GTP, pH 7.2-7.4, 275-285 mOsm. Picrotoxin (100 µm) was added to the aCSF to block $GABA_A$ receptor-mediated IPSCs. In addition, random experiments were performed with an internal solution added with biocytin (0.2%) to allow for subsequent immunocytochemical detection of TH[37] (**supplementary Fig. 10e-g**). Series and input resistance were monitored continuously on-line with a 5 mV depolarizing step (25 ms). Data were filtered at 2 kHz, digitized at 10 kHz, and collected on-line with acquisition software (pClamp 10.2; Molecular Devices). Dopamine neurons from the lateral portion of the posterior VTA were identified according to the already published criteria[69]: cell morphology and anatomical location (i.e., medial to the medial terminal nucleus of the accessory optic tract; **supplementary Fig. 10a,b**), slow pacemaker-like firing rate (<5 Hz), long action potential duration (>2 ms; **supplementary Fig.10d**), and the presence of a large I_h current (>150 pA[58]), which was assayed immediately after break-in, using 13 incremental 10 mV hyperpolarizing steps (250 ms) from a holding potential of −70 mV (**Supplementary Fig. 10c**). Putative GABA neurons of the lateral VTA were identified by their morphology, the absence of I_h and a short action

potential duration (>2 ms) (**Supplementary Fig. 10h,i**). In addition, random experiments were performed with an internal solution added with biocytin (0.2%) to allow for subsequent immunocytochemical detection of TH[37], since GABA cells are TH negative (**supplementary Fig. 10j-l**).

Spike fidelity was measured as the reliability to elicit an action potential in response to somatically injected current (50-200 pA): the jitter, which is equal to the standard deviation of the latency to elicit the first action potential, inversely correlates with spike fidelity as the smaller the jitter the higher degree of temporal precision exhibited by the cell. A bipolar, stainless steel stimulating electrode (FHC) was placed ~100-200 μm rostral to the recording electrode and was used to stimulate at a frequency of 0.1 Hz. Paired stimuli were given with an interstimulus interval of 50 ms, and the ratio between the second and the first PSCs (PSC2/PSC1) was calculated and averaged for a 5 min baseline[59]. NMDA EPSCs were evoked while holding cells at +40 mV. The AMPA EPSC was isolated after bath application of the NMDA antagonist D-AP5 (100 μM). The NMDA EPSC was obtained by digital subtraction of the AMPA EPSC from the dual (AMPA+NMDA-mediated) EPSC [60]. The values of the AMPA/NMDA ratio may be underestimated since the experiments were performed in the presence of spermine in the recording pipette. The spontaneous miniature EPSCs (mEPSCs) and IPSCs (mIPSCs) were collected in the presence of lidocaine (500 μM) or TTX (1 μM) and analyzed (120 sweeps for each condition, 1 sec/sweep) using Mini Analysis program (Synaptosoft, Decatur, GA). To accurately determine the minis amplitude, only events that were >8 pA were accepted for analysis (rise time <1 msec, decay time <3 msec). The choice of this cutoff amplitude for acceptance of minis was made to obtain a high signal-to-noise ratio. Then, each event was also visually inspected to prevent noise disturbance of the analysis. Experiments were performed blind to the experimental group.

Immunostaining. For a detailed protocol see Barna et al. [61] Rats were transcardially perfused with 4% (m/v) PFA or immersion-fixed in 4% PFA overnight and 20, 40 or 50 μm-thick sections of the midbrain were cut using a Leica VT-1000S Vibratome in phosphate buffer (PB). Immunostaining was performed in a free-floating manner. After extensive washing in PB and 0.05 M Tris-buffered saline (TBS, pH = 7.4), slices were blocked and permeabilized with 5% (v/v) Normal Donkey Serum (NDS, Sigma) and 0.3% (v/v) Triton X-100 (Sigma) in TBS for 45 min, then they were incubated in primary antibodies (see Table 1) in TBS while rinsed on an orbital shaker. Sections were then washed in TBS and incubated with the appropriate secondary antibodies (see Table 1) supplemented with DAPI (1:1000), if needed, then extensively washed in TBS and PB.

For confocal imaging sections were mounted in VectaShield (Vector Laboratories) or Prolong Diamond (Invitrogen) Antifade Mounting Medium. Confocal imaging was performed on the samples, and tyrosine hydroxylase (TH) -positive cell density and TH-immunofluorescence intensity were calculated on the images within the region of interest (ROI). vGluT1 and VIAAT inputs of the filled DAergic cells were counted in a ~1um neighborhood of the cells and input density was calculated based on the surface of the processes. Objects with a volume lower than 0.02 μm^3 were considered as noise and excluded from the analysis.

For STORM imaging sections were post-fixed in 4% PFA for 10 min and washed in PB. Samples were then mounted and dried on acetone-cleaned #1.5 borosilicate coverslips.

Correlated confocal and STORM imaging. Samples were covered with freshly prepared STORM imaging medium as previously described[62] and containing: 0.1 M mercaptoethylamine, 5% (m/v) glucose, 1 mg ml-1 glucose oxidase and catalase (2.5 μl/ml of aqueous solution from Sigma, approximately 1,500 U ml-1 final concentration) in Dulbecco's PBS (Sigma). Coverslips were sealed with nail polish. Imaging started after 10

minutes and was performed for up to 3 hours. Images were acquired by a Nikon Ti-E inverted microscope equipped with a Nikon N-STORM system, CFI Apo TIRF 100× objective (1.49 NA), a Nikon C2 confocal scan head and an Andor iXon Ultra 897 EMCCD (with a cylindrical lens for astigmatic 3D-STORM imaging[63]). Nikon NIS-Elements AR software with N-STORM module was used to control the imaging process. A 300-mW laser (VFL-P-300-647, MPB Communications) fiber-coupled to the laser board of the microscope setup was used for STORM imaging. The field of view was selected using the live EMCCD image with a 488-nm illumination and VIAAT-positive axon terminals impinging on TH-positive cell bodies and dendrites were selected. A three-channel confocal stack (512 × 512 × 15 pixels, 78 × 78 × 150 nm resolution) was then collected using 488-nm, 561-nm, and 647-nm excitations. After brief bleaching, direct STORM imaging was performed with 10,000 cycles of 30 ms exposure, with continuous low-power activator laser (405 nm) and maximal power reporter laser (647 nm) using a STORM filter cube (Nikon) and the EMCCD camera.

Correlated confocal and STORM image processing. Confocal image stacks were deconvolved with 100 iterations of the Classic Maximum Likelihood Estimation algorithm in Huygens software (SVI). STORM image processing was performed using the N-STORM module of the NIS-Elements AR. The peak detection threshold was set to 1,000 gray levels. Correlated confocal and STORM image analysis was performed using the VividSTORM software[61]. The data from the two imaging modalities were aligned manually based on the correlated STORM and confocal channels. One axon terminal was selected per image from the center of the field of view. The borders of the axon terminals and the outline of the active zones (for CB1 STORM and bassoon STORM, respectively) were delineated by the Morphological Active Contour Without Edges (MACWE) algorithm[77] using the appropriate confocal channels. STORM localization points (LPs) belonging to the

ROI were stored and counted and were normalized to the overall density of LPs per image. Size of the active zone was determined from the active contour ROIs, and the density of bassoon staining in the active zone was calculated by the division of bassoon number of LPs and the active zone size. Size of the axon terminals was also determined with the MACWE method using the VIAAT confocal channel, and the sum intensity of the VIAAT confocal staining was calculated in the ROIs to estimate transporter levels. Figures were prepared using Photoshop CS5 (Adobe Systems). All images were modified in the same way for all treatment groups during preparation of the figures to ensure equal comparison.

Statistical analysis. No statistical methods were used to predetermine the number of animals and cells required. Sample sizes were estimated based on previous experience and are similar to those reported in previous publications[37, 64, 65] and generally employed in the field. The animals were randomly assigned to each group at the prenatal pharmacological treatment or behavioral tests. Statistical analysis was conducted with GraphPad Prism 6 (San Diego). Statistical outliers were identified with the Grubb's test (α=0.05) and excluded from the analysis. Data sets were tested for normality using Kolmogorov-Smirnov test and differences between animals within a treatment group using Kruskal-Wallis test to determine the appropriate statistical method. For STORM imaging mean values of each animals were used in the statistics, differences between the groups were determined using Mann-Whitney U-test. Data always met the assumptions of the applied statistical probes. Electrophysiological data were analyzed by using two-way ANOVA for repeated measures (treatment × time), or one-way ANOVA or Student's t test when appropriate, followed by Sidak's, Dunnett's or Bonferroni's post hoc test. Behavioral parameters were analyzed by one-way or multiway ANOVAs followed by Tukey or Fisher LSD's test for post hoc comparisons. Correlation analyses were conducted by Pearson

correlation coefficient. The significance threshold was set at 0.05. Data collection and analysis were performed blind to the conditions of the experiments.

The datasets generated and analyzed during the current study are available from the corresponding author on reasonable request.

Online content

Any methods, additional references, Nature Research reporting summaries, source data, statements of code and data availability and associated accession codes are available at …

Methods-only references

51. Capone, F., Bonsignore, L.T. & Cirulli, F. Methods in the analysis of maternal behavior in the rodent. *Curr Protoc Toxicol* **Chapter 13**, Unit13 19 (2005).
52. Frau, R.*, et al.* Sleep deprivation disrupts prepulse inhibition of the startle reflex: reversal by antipsychotic drugs. *Int J Neuropsychopharmacol* **11**, 947-955 (2008).
53. Godar, S.C.*, et al.* Maladaptive defensive behaviours in monoamine oxidase A-deficient mice. *Int J Neuropsychopharmacol* **14**, 1195-1207 (2011).
54. Frau, R.*, et al.* The Neurosteroidogenic Enzyme 5alpha-Reductase Mediates Psychotic-Like Complications of Sleep Deprivation. *Neuropsychopharmacology* (2017).
55. Bortolato, M., Godar, S.C., Davarian, S., Chen, K. & Shih, J.C. Behavioral disinhibition and reduced anxiety-like behaviors in monoamine oxidase B-deficient mice. *Neuropsychopharmacology* **34**, 2746-2757 (2009).
56. Paxinos G, W.C. *The rat brain in stereotaxic coordinates* (Academic Press, San Diego, CA, 2007).
57. Devoto, P., Flore, G., Longu, G., Pira, L. & Gessa, G.L. Origin of extracellular dopamine from dopamine and noradrenaline neurons in the medial prefrontal and occipital cortex. *Synapse* **50**, 200-205 (2003).
58. Johnson, S.W. & North, R.A. Two types of neurone in the rat ventral tegmental area and their synaptic inputs. *J Physiol* **450**, 455-468 (1992).
59. Melis, M., Camarini, R., Ungless, M.A. & Bonci, A. Long-lasting potentiation of GABAergic synapses in dopamine neurons after a single in vivo ethanol exposure. *J Neurosci* **22**, 2074-2082 (2002).
60. Ungless, M.A., Whistler, J.L., Malenka, R.C. & Bonci, A. Single cocaine exposure in vivo induces long-term potentiation in dopamine neurons. *Nature* **411**, 583-587 (2001).
61. Barna, L.*, et al.* Correlated confocal and super-resolution imaging by VividSTORM. *Nat Protoc* **11**, 163-183 (2016).
62. Dani, A., Huang, B., Bergan, J., Dulac, C. & Zhuang, X. Superresolution imaging of chemical synapses in the brain. *Neuron* **68**, 843-856 (2010).
63. Huang, B., Jones, S.A., Brandenburg, B. & Zhuang, X. Whole-cell 3D STORM reveals interactions between cellular structures with nanometer-scale resolution. *Nat Methods* **5**, 1047-1052 (2008).
64. Dudok, B.*, et al.* Cell-specific STORM super-resolution imaging reveals nanoscale organization of cannabinoid signaling. *Nat Neurosci* **18**, 75-86 (2015).
65. Melis, M.*, et al.* PPARalpha Regulates Cholinergic-Driven Activity of Midbrain Dopamine Neurons via a Novel Mechanism Involving alpha7 Nicotinic Acetylcholine Receptors. *J Neurosci* **33**, 6203-6211 (2013).

Acknowledgements

We thank R. Tonini and O.J. Manzoni for discussions and comments on the manuscript. We thank G. Talani, M. Pignatelli, M. Tuveri, S. Aramo, G. Giua and B. Tuveri for their skillful assistance. The authors are also grateful to L. Barna for his help with STORM microscopy images, and thank Nikon Europe B.V., Nikon Austria GmbH and Auro-Science Consulting Ltd for kindly providing microscopy support. The present study was supported by University of Cagliari (RICCAR 2017 and 2018 to MM), Region of Sardinia (RASSR32909 to MM, and F72F16002850002 to RF), Fondazione Banco di Sardegna (F71I17000200002 to RF), European Molecular Biology Organization (ASTF 371-2016 to CS), Fondazione Zardi Gori (to CS), National Institute of Health (R01DA022340 to JFC, R01NS099457 to IK, and R01DA044925 to JFC, MM, IK), the Hungarian Academy of Sciences Momentum Program (LP-54/2013 to IK), the National Research, Development and Innovation Office of Hungary (VKSZ-14-1-2015-0155 to IK). The project was also funded by the Ministry of National Economy for STORM super-resolution microscopy (VEKOP-2.3.3-15-2016-00013 to IK). The authors also declare no competing financial interests.

Authors contribution

R.F. and F.T. designed and performed behavioral experiments and analyzed the data. S.F. and V.S. carried out behavioral observations. F.T. and V.S. prepared the figures. V.M. and C.I.P. carried out confocal imaging and STORM experiments, the corresponding data analysis and prepared the figures. P.S. and P.D. carried out cerebral microdialysis experiments and analyzed the data. M.C. and V.S. designed and performed maternal observation experiments. C.S., V.S. and S.A. performed chronic drug administration treatment. S.A. performed DREADD experiments. J.F.C. designed the DREADDs

853 experiment and contributed to manuscript preparation. I.K. designed confocal and STORM
854 experiments, analyzed and supervised imaging data and wrote the manuscript. M.M.
855 conceived, designed and supervised the project, performed patch-clamp recordings,
856 analyzed the data, prepared the figures and wrote the manuscript.

857

858 **Figure Legends**

859 **Figure 1. PCE elicits behavioral susceptibility to THC in male rat offspring.** THC (2.5
860 mg kg-1, s.c.) induces sensorimotor-gating deficits in male (**a**), but not female (**b**),
861 progenies as measured by PPI index (males, PCE-VEH vs PCE-THC: *P=0.037; CTRL-
862 VEH: n= 14; PCE-VEH, PCE-THC: n= 18; CTRL-THC: n= 17; females: P=0.44 between
863 groups; CTRL-VEH: n= 8; PCE-VEH: n= 9; CTRL-THC: n=7; PCE-THC: n= 11). (**c**) THC
864 induces larger dopamine (DA) increase in PCE nucleus accumbens (NAc) shell (*P<0.05
865 between groups; Sidak's test). Data represent mean ± S.E.M. Inset indicates DA basal
866 values, pg/sample (P= 0.205; two-tailed unpaired t-test; n= 7 per group). (**d**) PPI% values
867 inversely correlate with NAc DA levels of THC-treated PCE offspring. Data are fit by linear
868 regression (r2 = 0.62, P=0.01; CTRL: n= 11, PCE: n= 9). (**e**) DA synthesis inhibition by
869 alpha-methyl-para-tyrosine (AMPT, 200 mg Kg-1, i.p.) prevents THC-induced PPI deficits
870 in PCE progeny (***P=0.0008, PCE-VEH-THC vs PCE-AMPT-THC; CTRL-VEH-THC,
871 PCE-VEH-THC: n= 10 per group, CTRL-AMPT-THC: n= 9, PCE-AMPT-THC: n= 13). (**f**)
872 THC induces hyperlocomotion in PCE offspring (***P=0.0008, CTRL-VEH vs CTRL-THC:
873 n= 8 per group, PCE-VEH: n= 11, PCE-THC: n= 10). (**g**) Gi activation prevents THC-
874 induced hyperlocomotion in PCE offspring (*P<0.05, PCE-VEH vs PCE-THC; **P=0.003,
875 PCE-THC vs PCE-Gi-THC; PCE-VEH, PCE-Gi-VEH: n= 5 rats per group, PCE-THC: n= 8,
876 PCE-Gi-THC: n= 7). Distance travelled is percentage of activity compared to reference
877 group. (**h**) Crossing latency (***P=0.0006, PCE vs CTRL), and (**i**) number of stretched-

878 attend postures (SAPs) (**P<0.01, CTRL-VEH vs CTRL-THC; ***P<0.001, CTRL-VEH vs
879 PCE-VEH) are decreased in PCE offspring. THC does not modify latency to cross bridge
880 (h) (P=0.36, THC vs VEH group), but reduces SAPs number (i) only in CTRL (P=0.02,
881 THC vs VEH; CTRL-VEH: n= 8; CTRL-THC, PCE-THC: n= 8 per group, PCE-VEH: n= 10).
882 Unless otherwise indicated, graphs depict box-and-whisker plots (including minima,
883 maxima, and median values, and lower and upper quartiles) with single values. Data were
884 analyzed with two-way ANOVA followed by Tukey's test.

885

886 **Figure 2. PCE enhances pacemaker and evoked activity of VTA dopamine neurons**
887 **in male rat offspring.** (**a**) Representative traces of spontaneous activity of dopamine (DA)
888 neurons in acute slices from CTRL and PCE offspring (n= 20 and 21 experiments from
889 PCE and CTRL slices, respectively, were repeated independently with similar results
890 obtained). PCE offspring (nrat= 10, nlitter= 6) show (**b**) higher spontaneous activity (top,
891 **P=0.001 between groups; Welch's correction) and (**c**) lower resting membrane potential
892 (bottom, *P=0.01 between groups), compared to CTRL offspring (nrat= 10, nlitter= 6);
893 calibration bar: 100 ms, 20 mV. (d) PCE DA cells (nrat= 10, nlitter= 6) exhibit increased
894 excitability in response to current somatically injected (***P=0.0001 between groups; two-
895 way RM-ANOVA followed by Bonferroni) when compared to CTRL cells (nrat= 10, nlitter=
896 6). Data are represented as average values per animal ± S.E.M. Insets show
897 representative traces of evoked action potentials (APs) in response to maximum current
898 injected; calibration bar: 400 ms, 100 mV. (**e**) Quantification of the latency of first AP
899 appearance in response to the smallest current injected (***P<0.001 between groups).
900 Inset shows proportion of cells eliciting APs at 50 pA (CTRL in purple, PCE in blue). *Top*,
901 Representative traces of evoked APs in response to the minimum current injected;
902 calibration bar: 100 ms, 50 mV. (**f**) PCE DA cells exhibit a lower voltage threshold

(*P=0.015 between groups). (**g**) PCE does not affect after-hyperpolarization period (AHP) amplitude (P=0.47 between groups, ns) and (**h**) AHP duration (P=0.14 between groups, ns) of DA cells. Unless otherwise indicated, graphs show box-and-whisker plots (including minima, maxima, and median values, and lower and upper quartiles) with values averaged per animal and analyzed with two-sided unpaired t-test.

Figure 3. PCE reduces synaptic inhibition onto dopamine neurons in male rat offspring. (**a**) Traces (left) and plots (right) of evoked EPSCs and IPSCs recorded from same DA cells (**P=0.002 between groups; two-sided unpaired t-test; nlitter= 5 per group). n= 10 experiments from PCE and CTRL slices were repeated independently, with similar results obtained. (**b**) Input-output relationships (***P=0.0004 between groups) in CTRL and PCE DA cells. n= 5 and 8 experiments from CTRL and PCE slices were repeated independently, with similar results obtained. Data are represented as mean ± S.E.M. Left-hand panel shows IPSC traces; calibration bar: 5 ms, 100 pA. (**c**) PCE effect on inverse of squared coefficient of variation (1/CV2; ***P=0002 between groups) from (b). (**d**) Confocal image of VIAAT-containing terminals on a TH+-process. (**e**) Axon terminal from (d) decorated with bassoon-STORM number of localization points (NLPs) marking bouton active zone. n= 20 images per animal were acquired independently, with similar results obtained. (**f**) Bassoon density in VIAAT+ active zones (*P=0.030 between groups; two-sided Mann-Whitney U-test; nlitter= 4 per group). (**g**) IPSC traces recorded before and after (grey) WIN55.212-2 (WIN; 0.1 μM); calibration bar: 5 ms, 100 pA. (**h**) Dose-response curves for WIN displaying a larger (*P=0.01 between groups) and faster (**i**) effect (P=0.02 between groups) in PCE vs CTRL (nlitter= 4 per group). n= 8 and 6 experiments in PCE and CTRL were repeated independently, with similar results obtained. Average data per animal ± S.E.M. (**j**) CB1 NLP in VIAAT+ terminals (P=0.662 between groups; two-sided Mann-Whitney U-test; nlitter= 3 per group). n= 20 images per animal were acquired

928 independently, with similar results obtained. Unless otherwise indicated, graphs show box-
929 and-whisker plots (including minima, maxima, and median values, and lower and upper
930 quartiles) with values representing mean of averaged experiments per animal analyzed
931 with two-way RM-ANOVA followed by Bonferroni's test.

932 **Figure 4. Synaptic properties of excitatory inputs onto dopamine neurons are**
933 **affected by PCE in male rat offspring.** (**a**) PCE effects on input-output relationships
934 (****P<0.0001 between groups). n= 9 and 7 experiments from PCE and CTRL slices,
935 respectively, were repeated independently with similar results obtained. AMPA EPSC
936 traces are shown on the left. Data represent average values per animal ± S.E.M. (**b**) PCE
937 effect on inverse of squared coefficient of variation (1/CV2) from (a) (P=0.2 between
938 groups; two-sided Mann Whitney U-test). Data represent average values per animal ±
939 S.E.M. (**c**) Data from (a) and Figure 3a (nlitter= 5 per group) showing that AMPA EPSC
940 decay time kinetic (τ) do differ (***P=0.0004 between groups; two-sided unpaired t test). n=
941 15 and 17 experiments from PCE and CTRL slices, respectively, were repeated
942 independently, with similar results obtained. Insets show AMPA EPSC traces recorded at -
943 70 mV. (**d**) AMPA and NMDA EPSC traces recorded from DA neurons held at +40 mV; n=
944 9 and 10 experiments from PCE and CTRL slices, respectively, were repeated
945 independently, with similar results obtained. (**e**) PCE effect on AMPA/NMDA ratio
946 (****P<0.0001 between groups; two-sided unpaired t-test). (**f**) Cumulative frequency
947 distribution of AMPA/NMDA ratios (P=0.0002 between groups; two-sided Kolmogorov–
948 Smirnov test, D=1.0) recorded from CTRL (nrat= 6, nlitter= 4) and PCE rats (nrat= 7,
949 nlitter= 5). Unless otherwise indicated, graphs show box-and-whisker plots (including
950 minima, maxima, and median values, and lower and upper quartiles) with values
951 representing experiments averaged per animal and analyzed with two-way RM ANOVA.
952 Calibration bars: 10 ms, 50 pA.

Figure 5. PCE enhances post-synaptic responsiveness of dopamine neurons to excitatory stimuli in male rat offspring. (**a**) NMDAR EPSC decay time kinetic (weighted tau, τ) differs (****P<0.0001 between groups; two-sided unpaired t-test) between CTRL and PCE slices (nlitter= 6 per group). Box-and-whisker plots (including minima, maxima, and median values, and lower and upper quartiles) with circles representing average values per animal. n= 18 and 20 experiments from PCE and CTRL slices, respectively, were repeated independently, with similar results obtained. (**b**) Bimodal distribution of NMDAR EPSCs τ. (**c**) Dose-response curves for GluN2A antagonist PEAQX (*P=0.011 between groups;). n= 6 experiments per group were repeated independently, with similar results obtained. (**d**) Current-voltage relationship (I–V) plot shows that PCE (nlitter= 4) affects linearity of I-V curves (+40mV: *P=0.02 between groups). (**e**) Traces of AMPA EPSCs recorded at -70 and +40 mV from DA neurons in CTRL and PCE offspring. n= 11 and 6 experiments from PCE and CTRL slices, respectively, were repeated independently with similar results obtained. Calibration bar: 10 ms, 50 pA. (**f**) Dose-response curves for GluA2A antagonist NASPM displaying a larger effect (***P=0.0002 between groups) in PCE (nlitter= 2) offspring. n= 6 experiments per group were repeated independently, with similar results obtained. (**g**) AMPA EPSCs traces recorded at -70 mV before and after pairing low-frequency presynaptic stimulation (LFS; 1 Hz) with postsynaptic membrane depolarization (-40 mV). Calibration bar: 5 ms, 100 pA. (**h**) LFS (1 Hz at the arrow) induces long-term potentiation (LTP) (****P<0.0001 between groups) in PCE offspring (nrat= 5), whereas CTRL DA neurons (nrat= 4) exhibit long-term depression (LTD). n= 7 and 5 experiments from PCE and CTRL slices, respectively, were repeated independently with similar results obtained. Unless otherwise indicated, data are represented as average of experiments per animal ± S.E.M. analyzed with two-way RM ANOVA.

Figure 6. Pregnenolone rescues synaptic plasticity, mitigates deficits in dopamine neuron activity and restores behavior in PCE male rat progeny. (**a**) Pregnenolone (PREG) treatment. (b) PREG effects on low-frequency presynaptic stimulation (LFS;1 Hz at the arrow) (P=0.02, PCE-VEH vs PCE-PREG). Thick lines represent effects from Figure 5g. Data represent mean per animal ± S.E.M. Insets show traces (-70 mV) from before (1) and after LFS (2); calibration bar: 5 ms, 100 pA. n= 6 experiments per group were repeated independently, with similar results obtained. (**c**) Effects of PREG on resting membrane potential (****P=0.0006, PCE-VEH vs PCE-PREG; **P<0.01, PCE-VEH vs CTRL-VEH; nlitter= 5 per group). (**d**) PREG effect on spontaneous activity (**P<0.01, PCE-VEH vs PCE-PREG; *P=0.02, PCE-VEH vs CTRL-VEH; nlitter= 5 per group). (**e**) Traces from PREG-treated offspring; calibration bar: 20 ms, 100 pA. n= 14 and 12 experiments from PCE and CTRL slices were repeated independently, with similar results obtained. (**f**) Multimodal distribution from (d). (g) Traces of evoked firing in PREG-treated offspring; calibration bar: 400 ms, 100 mV. N of experiments are as in (c-h). (**h**) PREG restores evoked firing (****P<0.0001, PCE-VEH vs PCE-PREG; nlitter= 5 per group). Data represent values averaged per animal ± S.E.M. (**i**) PREG attenuates THC effects on NAc DA levels in PCE rats (P=0.30 between groups). Thick lines are from Figure 1c. Data represent mean ± S.E.M. (**j**) Basal DA values (pg/sample) (P=0.768 between groups; two-sided unpaired t-test). (**k**) PREG prevents THC effects on PPI in PCE offspring (*P=0.032, PCE-THC-VEH vs PCE-THC-PREG; ***P=0.0004, CTRL-THC-VEH vs PCE-THC-VEH; Tukey's test; CTRL-THC-VEH: n=17; CTRL-THC-PREG, PCE-THC-VEH, PCE-THC-PREG: n= 16; nlitter=8 per group). Unless otherwise indicated, box-and-whisker plots (including minima, maxima, and median values, and lower and upper quartiles) with circles depict average data per animal analyzed with two-way RM ANOVA followed by Sidak's test.

1003

1004

1005

1006

1007

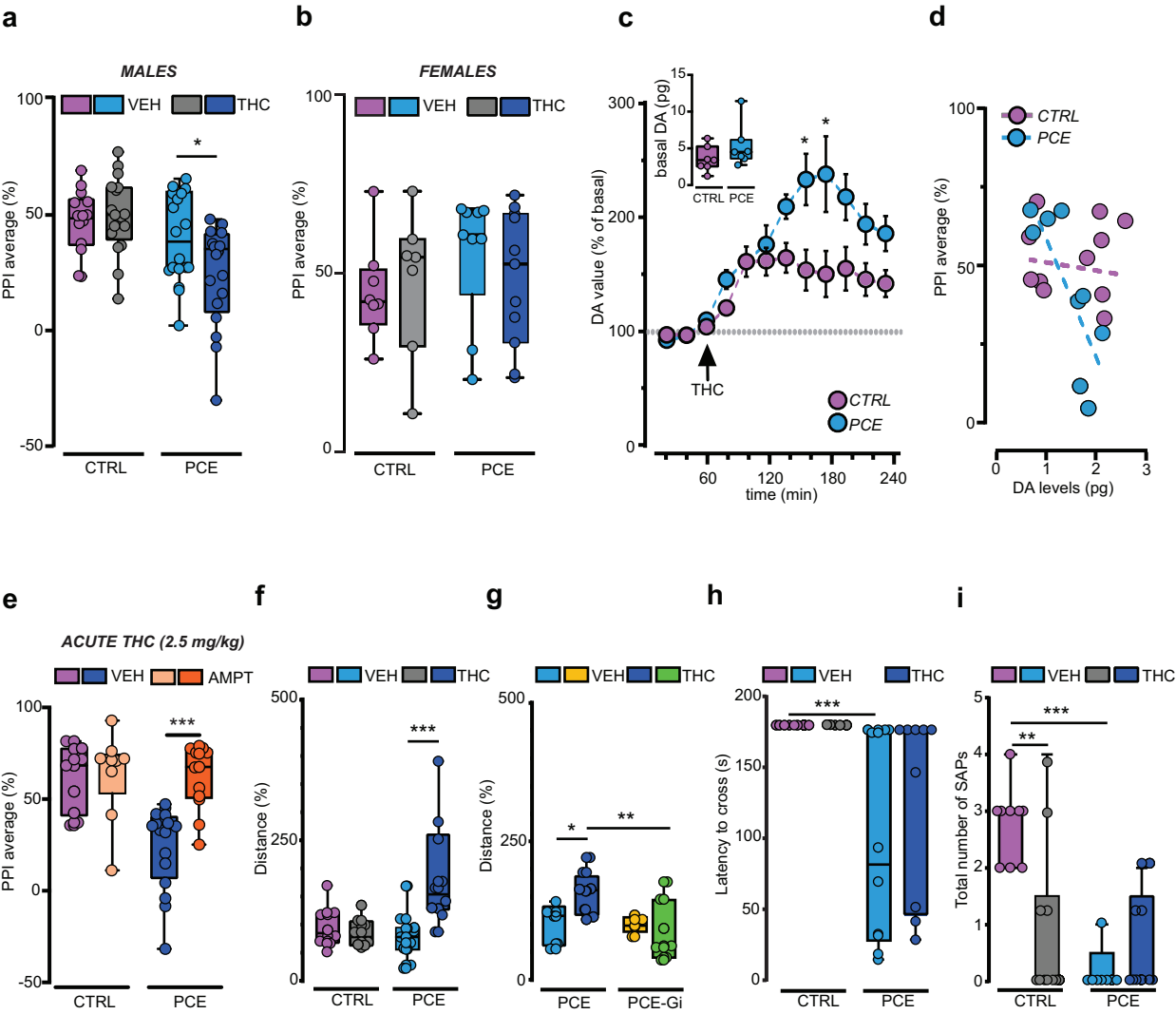
a
MALES
VEH
THC
PPI average (%)
CTRL
PCE
b
FEMALES
c
basal DA (pg)
DA value (% of basal)
THC
CTRL
PCE
time (min)
d
DA levels (pg)
e
ACUTE THC (2.5 mg/kg)
AMPT
f
Distance (%)
g
PCE-Gi
h
Latency to cross (s)
i
Total number of SAPs

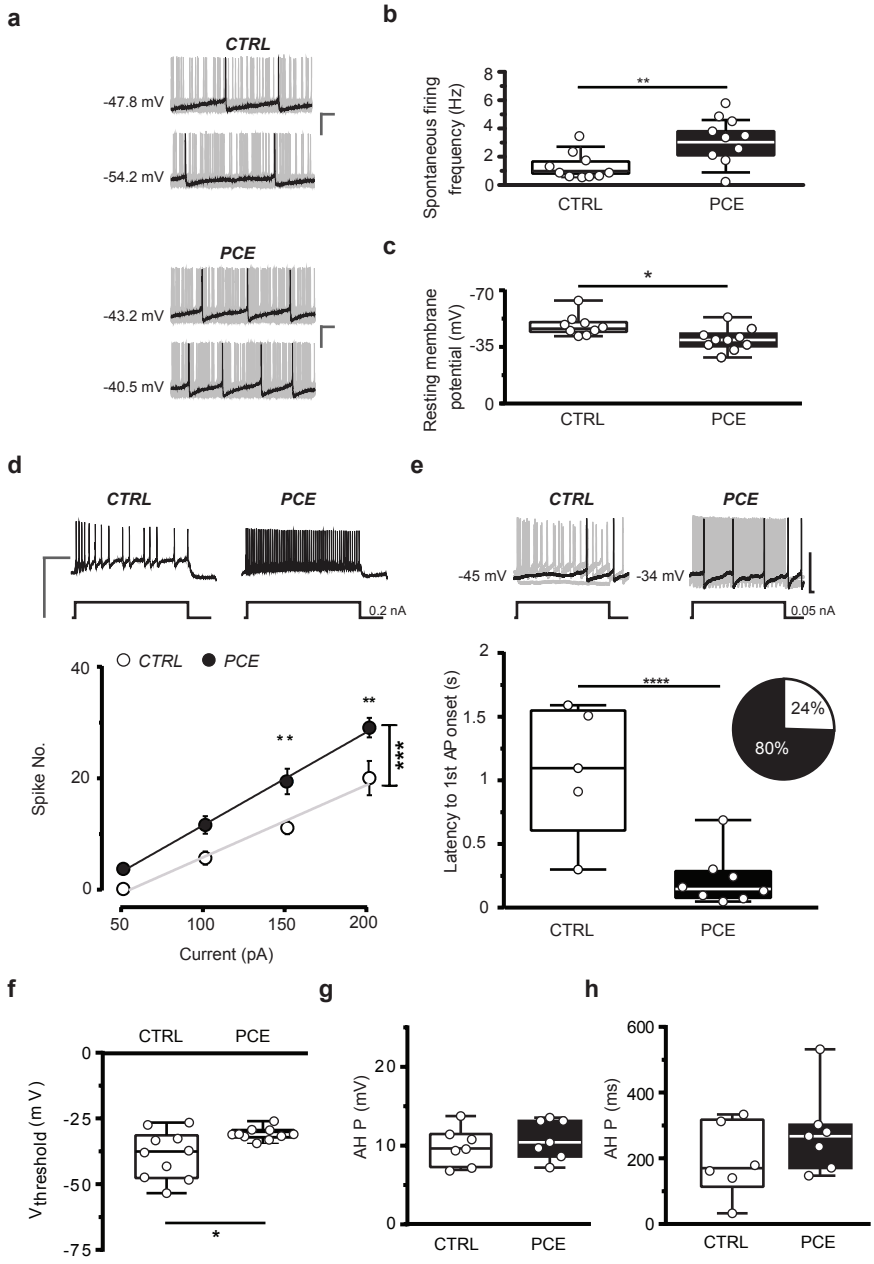
a
CTRL
-47.8 mV
-54.2 mV
PCE
-43.2 mV
-40.5 mV
b
Spontaneous firing frequency (Hz)
8
6
4
2
0
**
CTRL
PCE
c
Resting membrane potential (mV)
-70
-35
0
*
CTRL
PCE
d
CTRL
PCE
0.2 nA
CTRL
PCE
Spike No.
40
20
0
**
**
***
50
100
150
200
Current (pA)
e
CTRL
PCE
-45 mV
-34 mV
0.05 nA
Latency to 1st AP onset (s)
2
1.5
1
0.5
0
****
24%
80%
CTRL
PCE
f
CTRL
PCE
Vthreshold (m V)
0
-25
-50
-75
*
g
AH P (mV)
20
10
0
CTRL
PCE
h
AH P (ms)
600
400
200
0
CTRL
PCE

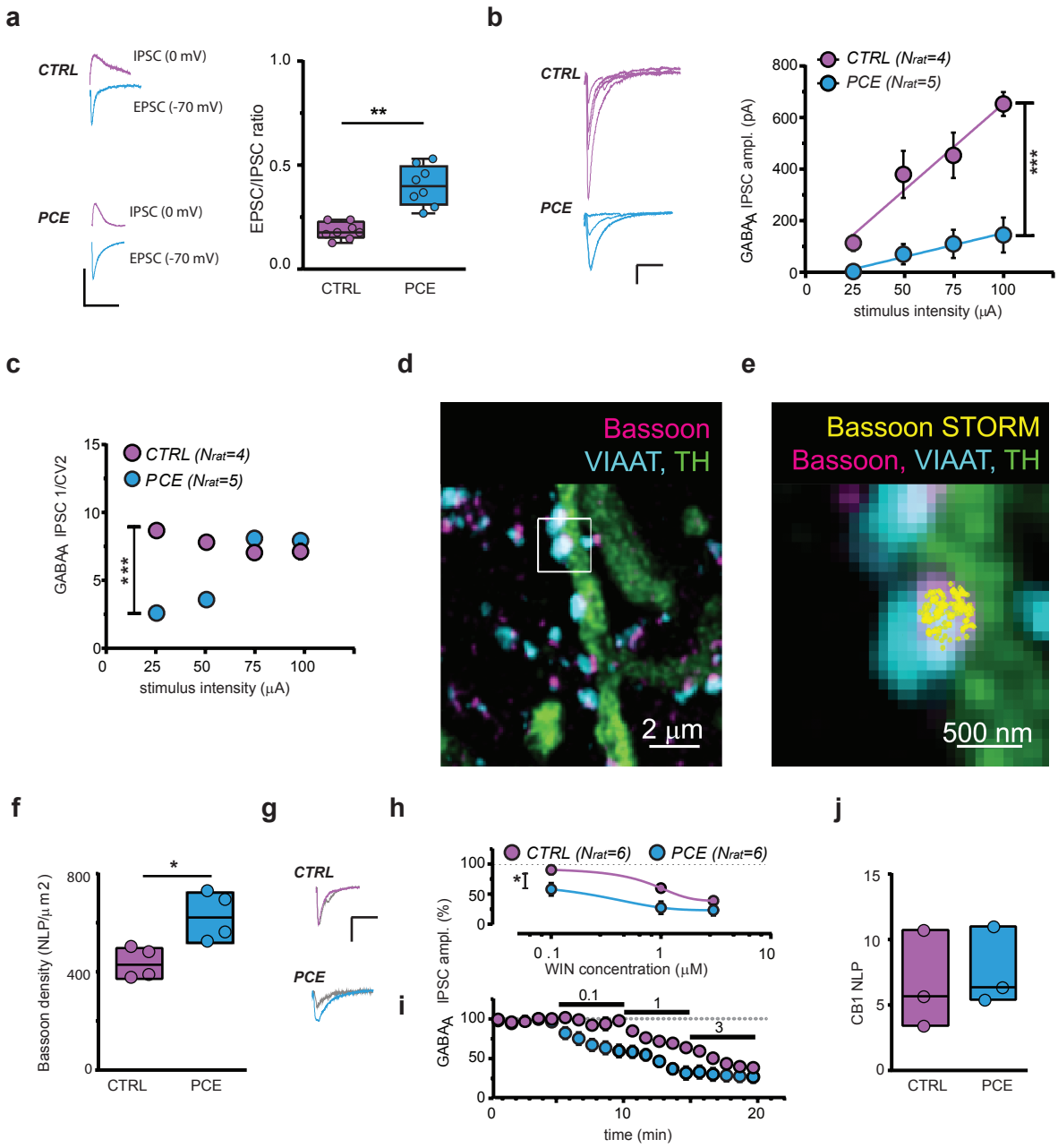
a
CTRL
IPSC (0 mV)
EPSC (-70 mV)
PCE
IPSC (0 mV)
EPSC (-70 mV)
EPSC/IPSC ratio
1.0
0.5
0.0
**
CTRL
PCE
b
CTRL
PCE
CTRL (Nrat=4)
PCE (Nrat=5)
GABAA IPSC ampl. (pA)
800
600
400
200
0
***
0
25
50
75
100
stimulus intensity (μA)
c
CTRL (Nrat=4)
PCE (Nrat=5)
GABAA IPSC 1/CV2
15
10
5
0
***
0
25
50
75
100
stimulus intensity (μA)
d
Bassoon
VIAAT, TH
2 μm
e
Bassoon STORM
Bassoon, VIAAT, TH
500 nm
f
Bassoon density (NLP/μm2)
800
400
0
*
CTRL
PCE
g
CTRL
PCE
h
CTRL (Nrat=6)
PCE (Nrat=6)
IPSC ampl. (%)
100
50
0
*
0.1
1
10
WIN concentration (μM)
i
GABAA
100
50
0
0.1
1
3
0
10
20
time (min)
j
CB1 NLP
15
10
5
0
CTRL
PCE

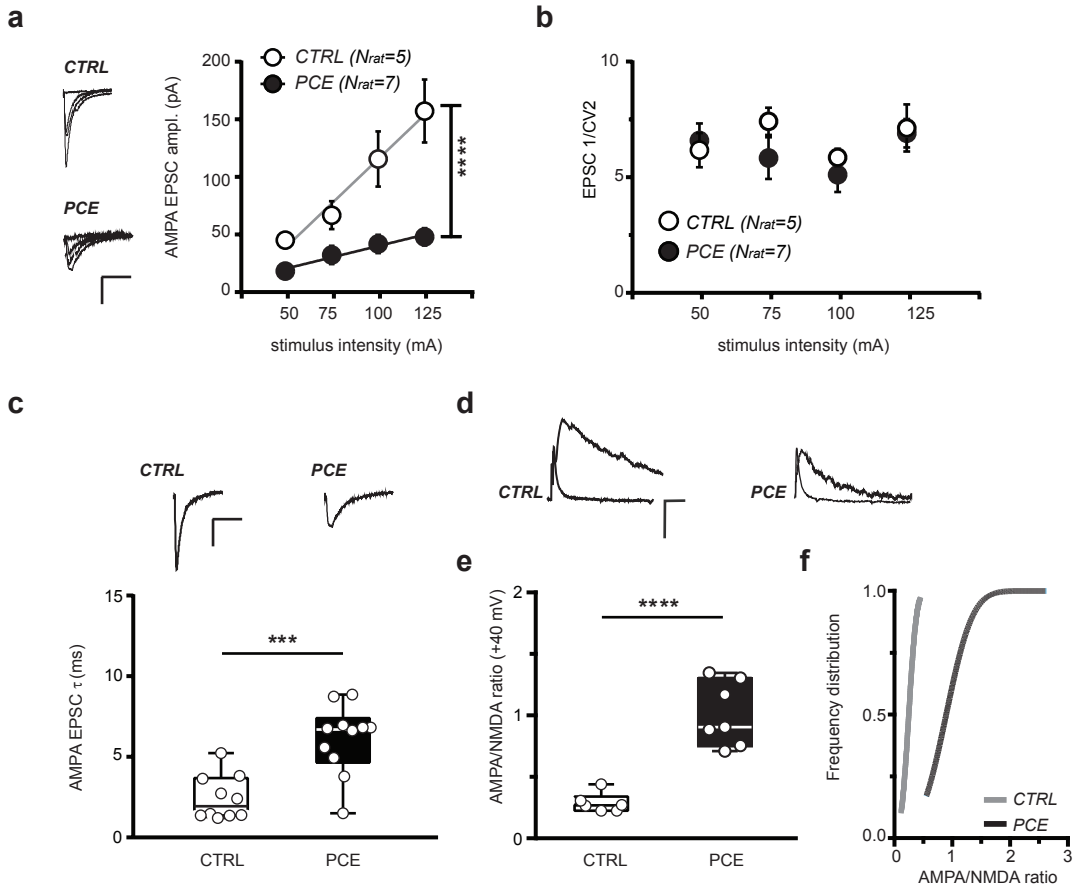
a
CTRL
PCE
CTRL (Nrat=5)
PCE (Nrat=7)
AMPA EPSC ampl. (pA)
200
150
100
50
0
****
50 75 100 125
stimulus intensity (mA)
b
EPSC 1/CV2
10
5
0
CTRL (Nrat=5)
PCE (Nrat=7)
50 75 100 125
stimulus intensity (mA)
c
CTRL
PCE
AMPA EPSC τ (ms)
15
10
5
0
***
CTRL
PCE
d
CTRL
PCE
e
AMPA/NMDA ratio (+40 mV)
2
1
0
****
CTRL
PCE
f
Frequency distribution
1.0
0.5
0.0
0 1 2 3
AMPA/NMDA ratio
CTRL
PCE

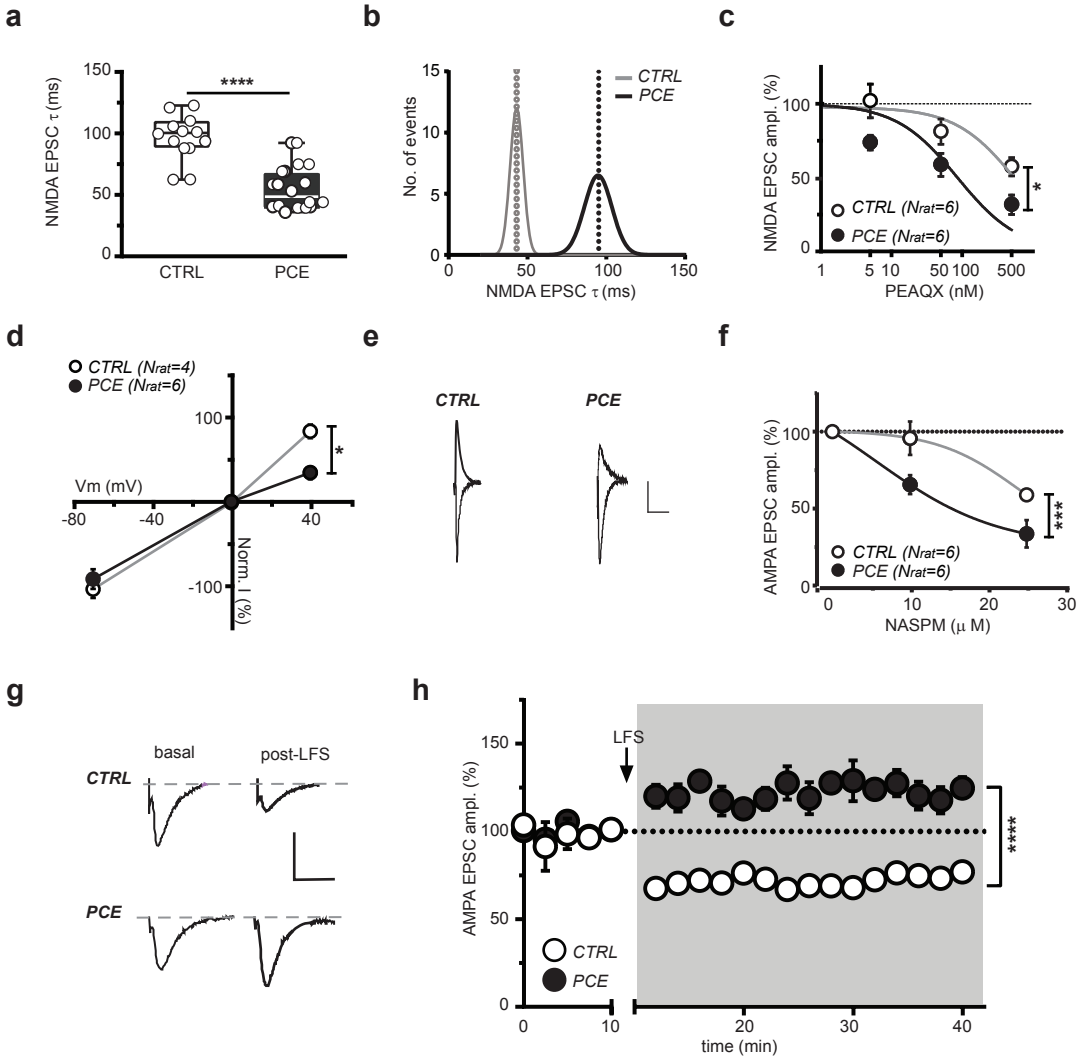
a
NMDA EPSC τ (ms)
150
100
50
0
****
CTRL
PCE
b
No. of events
15
10
5
0
CTRL
PCE
0
50
100
150
NMDA EPSC τ (ms)
c
NMDA EPSC ampl. (%)
100
50
0
CTRL (Nrat=6)
PCE (Nrat=6)
*
1
5
10
50
100
500
PEAQX (nM)
d
CTRL (Nrat=4)
PCE (Nrat=6)
100
-100
*
Vm (mV)
-80
-40
40
Norm. I (%)
e
CTRL
PCE
f
AMPA EPSC ampl. (%)
100
50
0
CTRL (Nrat=6)
PCE (Nrat=6)
***
0
10
20
30
NASPM (μ M)
g
basal
post-LFS
CTRL
PCE
h
LFS
AMPA EPSC ampl. (%)
150
100
50
0
CTRL
PCE
****
0
10
20
30
40
time (min)

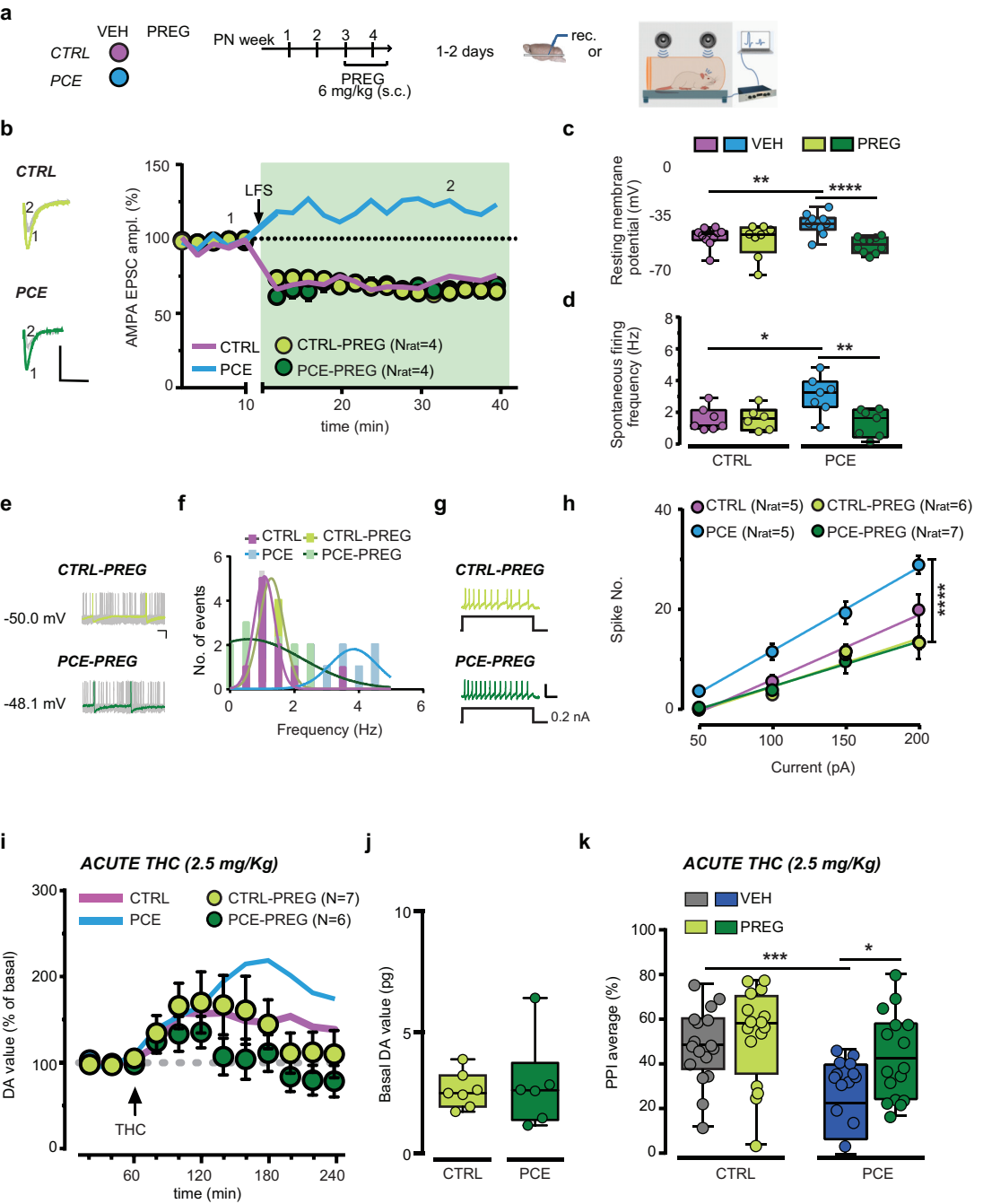
a
VEH
PREG
CTRL
PCE
PN week 1 2 3 4
PREG
6 mg/kg (s.c.)
1-2 days
rec.
or
b
CTRL
PCE
AMPA EPSC ampl. (%)
LFS
CTRL
PCE
CTRL-PREG (Nrat=4)
PCE-PREG (Nrat=4)
time (min)
c
VEH
PREG
Resting membrane potential (mV)
d
Spontaneous firing frequency (Hz)
CTRL
PCE
e
CTRL-PREG
-50.0 mV
PCE-PREG
-48.1 mV
f
CTRL
CTRL-PREG
PCE
PCE-PREG
No. of events
Frequency (Hz)
g
CTRL-PREG
PCE-PREG
0.2 nA
h
CTRL (Nrat=5)
CTRL-PREG (Nrat=6)
PCE (Nrat=5)
PCE-PREG (Nrat=7)
Spike No.
Current (pA)
i
ACUTE THC (2.5 mg/Kg)
CTRL
PCE
CTRL-PREG (N=7)
PCE-PREG (N=6)
DA value (% of basal)
THC
time (min)
j
Basal DA value (pg)
CTRL
PCE
k
ACUTE THC (2.5 mg/Kg)
VEH
PREG
PPI average (%)
CTRL
PCE